Peer-Reviewed Technical Communication

HF Radar Real-Time Alert to a Tsunami-Like Disturbance at Tofino on January 5, 2020: Surge or Tsunami?

Mal Heron, *Life Fellow, IEEE*, Baptiste Domps, Charles-Antoine Guérin, Manman Wang, and Leif Petersen

***Abstract*—A real-time alert issued by a high frequency (HF) Wellen radar (WERA) at Tofino on January 5, 2020 was identified as a possible meteotsunami because of the anomalous surface currents. Reanalysis of the HF radar data and consideration of associated meteorological data from Global Forecast System North West Pacific forecasts, the GOES-17 weather satellite and the NDBC buoy at La Pérouse, indicate that the anomaly in ocean currents was a combination of a wind setup at the coast over several preceding hours and an abrupt change in wind direction driven by the passage of a severe cold front. It is unlikely that the Proudman resonance condition between the wind speed and gravity wave phase velocity existed, except perhaps very close to the coast. The inclusion of the wind direction measurements by the HF radar will improve the real-time alerts at the coast by discriminating between tsunamis and wind-driven storm surge events.**

***Index Terms*—HF radar, storm surges, surface currents, tsunamis, wind directions.**

I. Introduction

HF OCEAN radar technology is well established with over 400 systems worldwide predominantly deployed to measure surface currents in the coastal zone 5–200 km from the shore [1], [2]. Surface currents are generally presented on a rectangular grid with resolutions varying from about 500 m to 20 km depending on the operating frequency of the radar, the range, and the type of radar being used. The normal practice for archiving surface current data is hourly samples averaged over 1–3 h. Phased-array type of HF ocean radars has the additional capability of routinely mapping wind directions on the same grid but with reduced range for wave heights because the second-order part of the echo spectrum is used. It has been shown [3] that with good signal-to-noise ratios, the echo spectrum of phased-array ocean radars can be inverted to produce full directional wave spectra. It has been demonstrated that HF radars can be used to observe the presence of earthquake-generated tsunamis in the relatively shallow coastal waters [4], [5], [6], as well as observations of meteotsunamis, and simulation studies [7], [8], [9]. The Wellen radar (WERA) phased array system produces real-time alerts for tsunami-like disturbances in coastal ocean waters. The purpose of this article is to refine the analysis to differentiate between tsunamis and other disturbances in the ocean and focus on the tsunami-like event on January 5, 2020 at Tofino, British Columbia (BC). A similar event at Tofino on October 14, 2016 was analyzed by a fast Fourier transform method [10], and also by a time-correlation analysis [11] showing that the disturbance had characteristics of a meteotsunami.

HF ocean radars are used to measure surface current components in the radial direction from the station by measuring the Doppler shift on first-order Bragg lines in the echo spectrum. The theory and practice of this analysis is well established and useful reviews are given in [1], [2], and [12], and their reference lists. The main feature is that the Doppler shifts of the first-order spectral peaks are given by

$$\Delta f = \pm\sqrt{\frac{g}{2\pi\lambda}} - \frac{v}{\lambda} \tag{1}$$

where λ is the wavelength of the Bragg wave on the ocean and v is the surface current component in the radial direction. The positive option in (1) is for the Doppler shift of the Bragg wave approaching the radar and the negative is for the receding wave. In (1), λ is exactly half the wavelength of the electromagnetic radar wavelength so the relationship between Δf and v is simply linear and defined by the radar operating frequency.

For coastal circulation applications, two radar stations are normally deployed so that they can measure radial components of velocity in target pixels on the sea at different angles. From those two radial components, the surface current vector can be calculated. Most HF radar installations have been made for circulation monitoring in coastal waters and the normal archiving practice is for hourly sampling of east and north components on a rectangular grid. Special sampling strategies are needed for tsunami detection because the expected period for tsunami waves is 10–40 min, so the time series sampling must be less than the Nyquist limit of 5 min, and spatial integration has to be significantly less than the expected wavelengths.

II. HF Radar Detection of Tsunamis

Tsunamis are shallow water gravity waves, even in the deepest oceans. The dispersion equation is

$$c = \sqrt{gd} \tag{2}$$

where d is the water depth and g is gravitational acceleration.

In the deep ocean of, say, 3000 m, the phase velocity of a tsunami is about 170 m·s^{-1} and wavelengths are in the order of 200 km, but in coastal waters the velocity is typically 30 m·s^{-1} with wavelengths tens

Manuscript received 31 January 2022; revised 9 March 2023; accepted 18 April 2023. Date of publication 12 October 2023; date of current version 8 February 2024. The Ocean Networks Canada was supported in part by the Canada Foundation for Innovation and in part by the Department of Fisheries and Oceans of Canada. The WERA radar was supported by Western Economic Development. *(Corresponding author: Mal Heron.)*

Associate Editor: E. Gill.

Mal Heron is with Marine Geophysics Laboratory and Physical Sciences, James Cook University, Douglas, QLD 4811, Australia (e-mail: mal.heron@ieee.org).

Baptiste Domps is with the Degreane Horizon, 83390 Cuers, France, and also with the CNRS, IRD, MIO, Université de Toulon, Aix Marseille Université, 83130 Toulon, France (e-mail: baptiste.domps@degreane-horizon.fr).

Charles-Antoine Guérin is with the CNRS, IRD, MIO, Université de Toulon, Aix Marseille Université, 83130 Toulon, France (e-mail: guerin@univ-tln.fr).

Manman Wang is with the Ocean Networks Canada, The University of Victoria, Victoria, BC V8P 5C2, Canada (e-mail: manmanw@uvic.ca).

Leif Petersen is with Helzel Messtechnik GmbH, 24568 Kaltenkirchen, Germany (e-mail: petersen@helzel.com).

Digital Object Identifier 10.1109/JOE.2023.3269749

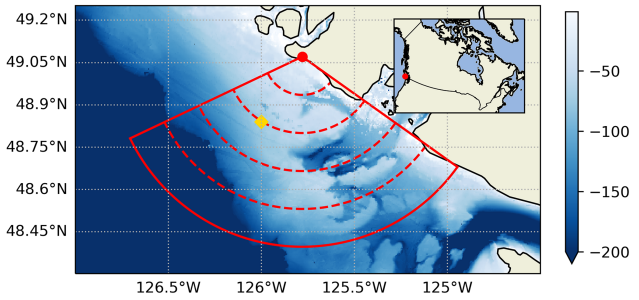

Fig. 1. WERA HF radar deployment at Tofino showing radar coverage (———) and range arcs at 30, 45, and 60 km (– – – –). The base map shows bathymetry on the color scale. The yellow dot marks the position of the NDBC buoy.

of kilometers. A simplified approach is given [13] for the transformation of amplitude of the deep-ocean tsunami as it propagates into the shallow coastal water. The water elevation is given by

$$h\ (d) = h\,(D)\left(\frac{D}{d}\right)^{1/4} \tag{3}$$

where D is a reference depth where the water elevation due to the tsunami is $h(D)$.

For a tsunami with maximum surge velocity v_m in water depth d, the amplitude is given [13] as

$$h\ (d) = v_m\left(\frac{d}{g}\right)^{1/2}. \tag{4}$$

There are two velocities to be understood in a tsunami wave. One is the phase velocity given by (2) and the other is the orbital velocity of parcels of water as the wave propagates. The latter is manifest on the surface as a to-and-fro movement of the water, and it is this surge velocity that is interpreted by the HF radar as a current. For the transformation from deep water D to shallow water d, the maximum surge velocity in the tsunami wave is described, as a consequence of (3) and (4) [14], by

$$v_m\ (d) = v_m\,(D)\left(\frac{D}{d}\right)^{3/4}. \tag{5}$$

As an example, the Andaman Island earthquake on December 24, 2004 produced a tsunami with water elevation of about 0.5 m in deep water (observed by the Jason-1 altimeter [15]), with $v_m = 0.03\,\mathrm{m{\cdot}s^{-1}}$. As it propagated onto a shelf of 100 m depth, the elevation was about 1.2 m and the maximum surge velocity was $0.37\ \mathrm{m{\cdot}s^{-1}}$. These are not typical figures; this was a major tsunami that caused significant damage and loss of life. It has been suggested [16] that an HF radar needs to be able to resolve an anomaly in surface current of less than $0.05\ \mathrm{m{\cdot}s^{-1}}$ to detect hazardous tsunamis near the coast and issue useful alerts.

III. Observations and Results

The layout of the WERA HF radar at 49° 4.9′ N, 125° 45.9′ W, and the National Data Buoy Center (NDBC) Buoy C46206, located at 48° 49.8′ N, 126° 00.0′ W, is shown in Fig. 1.

A. WERA Tsunami ALERT

The WERA phased-array station at Tofino is set up with the tsunami detection software provided by the manufacturer [8]. An integration time of 133 s was selected for WERA as a tradeoff between precision in

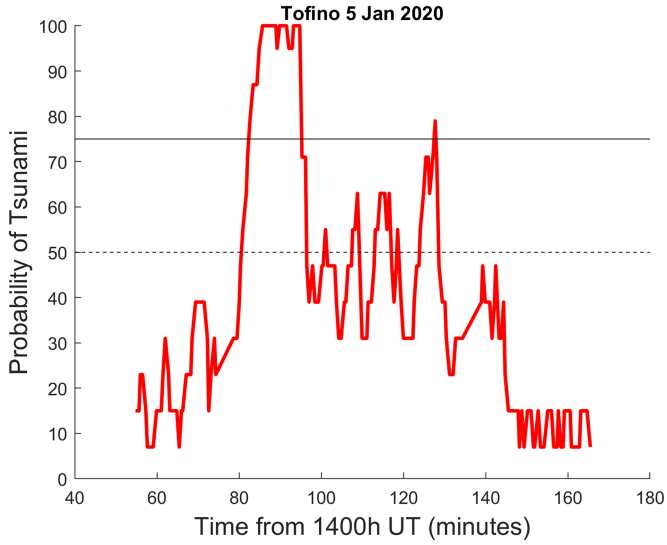

Fig. 2. Probability of a tsunami, issued automatically in real time by the WERA HF radar at Tofino. When the probability exceeds 75%, WERA issues an ALERT; between 50% and 75%, it issues an ATTENTION report.

surface currents and resolution of short-period tsunamis. Time series of length 133 s are extracted every 33 s from the continuous coherent sampling. At each 33-s time step, the recent 133-s time series is analyzed and radial components of surface currents are produced for each point on a rectangular grid. At each grid point, a moving polynomial regression spanning the previous 45–60 min is used to evaluate tidal currents (and other long-term current variations) and obtain radial current residuals [9]. The probability of a tsunami is estimated at each grid point every 33 s using a constant false alarm rate (CFAR) algorithm where the probability of a false alarm is determined by the likelihood that the noise or signal exceeds a given level [9].

The spatial pattern over the whole grid is assessed before the probability of tsunami (PT) is estimated. The summary real-time output of PT for the period of the alert at Tofino on January 5, 2020 is shown in Fig. 2. For PT $<$ 50, there is no warning; for 50 $<$ PT $<$ 75, the message is "ATTENTION"; and for PT $>$ 75, an "ALERT" is issued.

The initial ALERT period commenced at 15:22:39 h UT on January 5, 2020 and was centered on 15:28:45 h UT with subsequent minor peaks after 12.3, 19.8, 26.4, 38.6, and 52.2 min. This time series suggests an initial pulse on the ocean with a subsequent decaying wave train.

At each time point in Fig. 2, the single metric is derived from the map of tsunami probability levels at the grid points. A sample of maps is shown in Fig. 3, where the red color indicates greater than 70% likelihood of a tsunami at each individual grid point. The six panels in Fig. 3 cover the case at 15:16 h when the distribution of probabilities did not trigger a report, through the period when ATTENTION and ALERT messages were issued, and back to no trigger by 15:40 h.

There is a tendency for the active areas on the ocean in Fig. 3 to be rotated slightly from N-S toward north-west to south-east. The speed of the west-to-east movement of the disturbance was calculated from the radar probability maps in a latitude band that spanned the latitude of the NDBC buoy. The speed was $17.0 \pm 3.2\ \mathrm{m{\cdot}s^{-1}}$ with no significant acceleration.

B. Tides

The disturbance event identified by the HF radar occurred about 14 min before the predicted high tide at Tofino. A

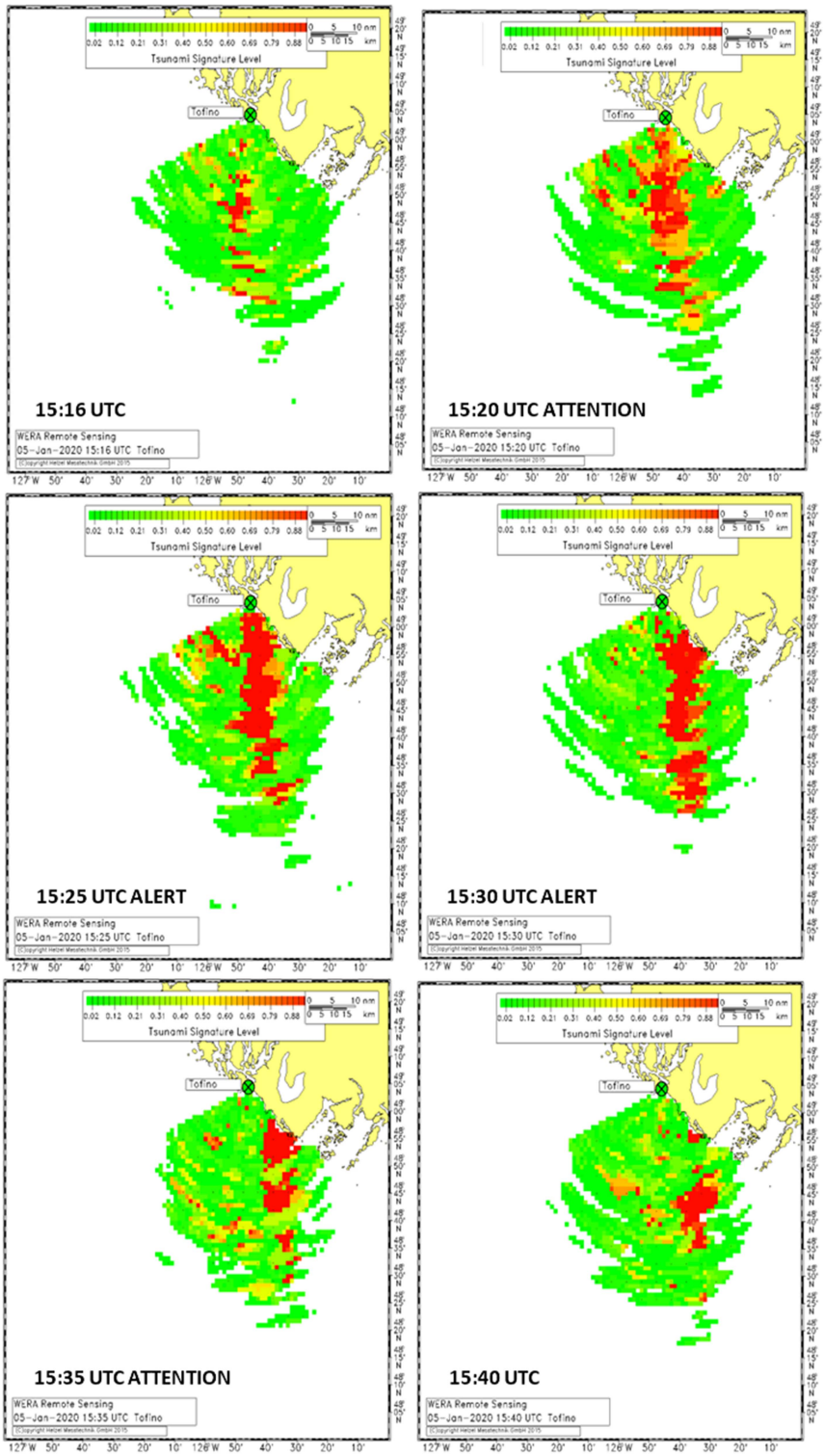

Fig. 3. Tsunami probability level at individual grid points at 5-min intervals through the disturbance period. Tsunami Signature Level shown is in PT/100. Images by permission of Helzel Messteknic GmbH.

consistent onshore wind over more than the previous 12 h had produced a surge where the water heights observed by the Tofino tide gauge were up to 12.7 cm above the astronomical prediction. Fig. 4(b) shows that the surge height reached a peak at 15:06 h nearly 17 min before the start of the radar alert. The maximum observed water height was 3.26 m at 14:52 h and the maximum predicted tide was 3.25 m at 15:08 h. Thus, the surge moved the peak of the tide some 16 min earlier than the predicted high water. Fig. 4(c) and (d) show that the peak of the tidal surge was close to simultaneity with the beginning of an anomalous southwards flow (residual current) observed by the HF radar at a distance 10 km

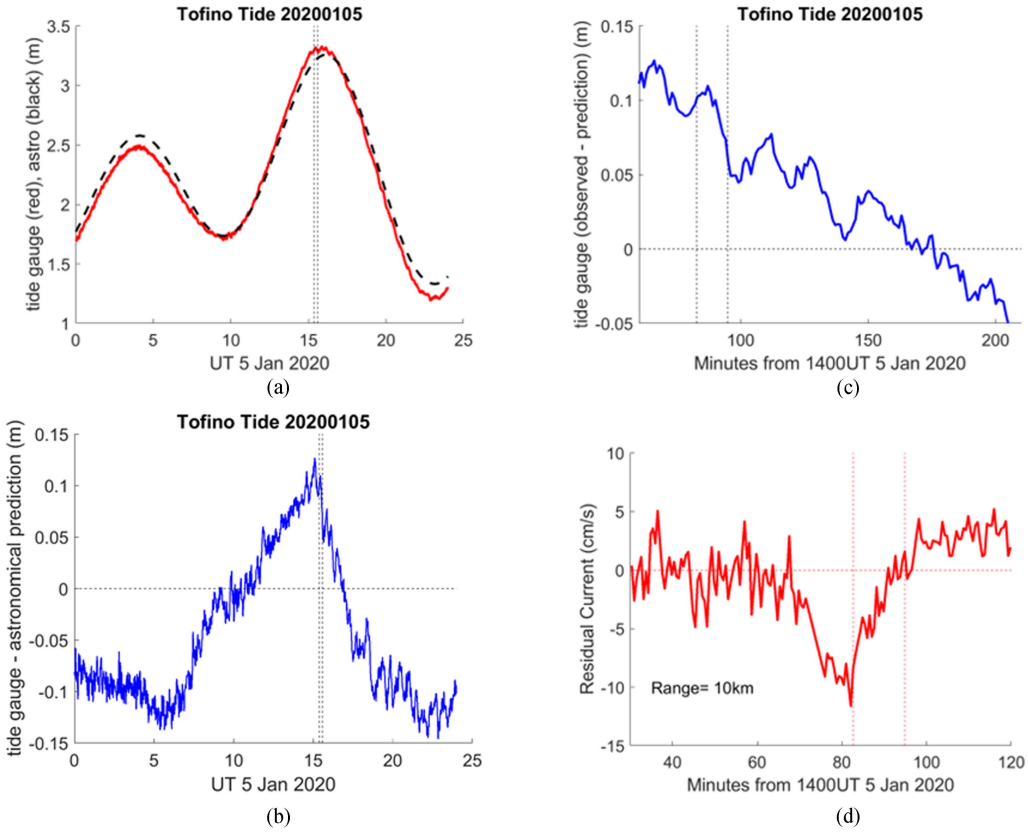

Fig. 4. Water level data from Tofino where the vertical dashed lines show the interval in which the HF radar issued an alert. (a) Solid red = the tide gauge at Tofino and dashed black = the astronomical prediction. (b) Difference is the surge caused by the wind. (c) Surge, expanded around the time of the radar alert. (d) Residual current (cm·s^{-1} positive north) from radar data.

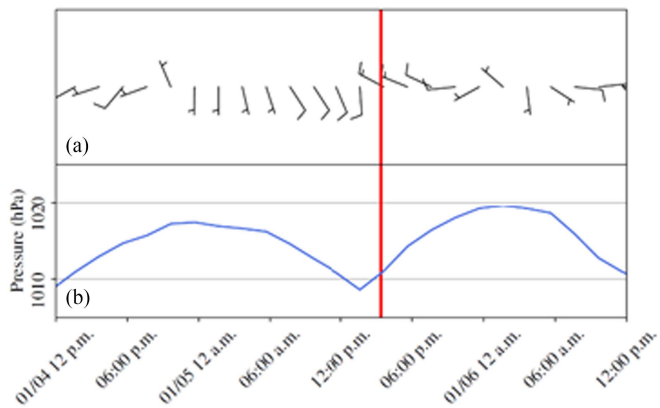

Fig. 5. Hourly atmospheric recordings from the La Pérouse bank buoy. (a) Barbs indicating 5-m wind speed (knots) and direction. (b) Atmospheric pressure (hPa). The time of the WERA tsunami alert is marked by ———.

south of the radar station. The main question arising here is about the cause of the anomaly in the current.

C. Atmospheric Disturbances and Their Propagation

1) Synoptic Analysis: The event of January 5, 2020 was characterized by a sudden drop in sea-level atmospheric pressure from 1017 to 1008 hPa over 12 h, as measured by the La Pérouse buoy (see Fig. 5) located by the yellow diamond in Fig. 1. The minimum pressure was measured at 13:38 and coincides with a drastic wind shear in direction (from north to south-west) and speed (from 5 to 15 knots). Notably, the passing of this strong atmospheric disturbance over the buoy happened about 1 h before the WERA tsunami alert.

At a synoptic scale, Global Forecast System (GFS) North West Pacific (see Fig. 6) shows a low-pressure cyclonic zone North of BC, moving east-south-east on January 4 and 5. The surrounding wind and pressure patterns are typical of a cold front, here propagating from the North-West toward BC. Divergence of the horizontal wind field is used as a marker of the cold front and reveals a narrow convergence area with intense vertical motion. The speed of this atmospheric disturbance is estimated to be 13.9 m·s^{-1} ($\pm$1.4 m·s^{-1}) between 00:00 and 12:00 [see Fig. 6(c)–(e)]. However, its exact motion off Tofino between 12:00 and 18:00 [see Fig. 6(e) and (f), respectively] cannot be inferred from GFS because of the 6-h temporal resolution.

2) Propagation of the Atmospheric Disturbance as Seen by Satellite: To better track the atmospheric process in the radar sweep area, we analyzed satellite images from the weather satellite GOES-17 having a 10-min temporal resolution, as suggested by Domps et al. [17]. The cold front position can be estimated from typical cloud features that yield a distinct signature in infrared imagery. As an example, Fig. 7 depicts the cloud-top brightness temperature derived from GOES-17 Advanced Baseline Imager (ABI) band 13 (10.3 μm) at 12:00. Colored pixels indicate convective clouds with high and cold tops advancing ahead of the front.

To further investigate the relationship between the propagating atmospheric turbulence and the variations in sea surface currents, we went through a systematic search of the cold front arrival time for

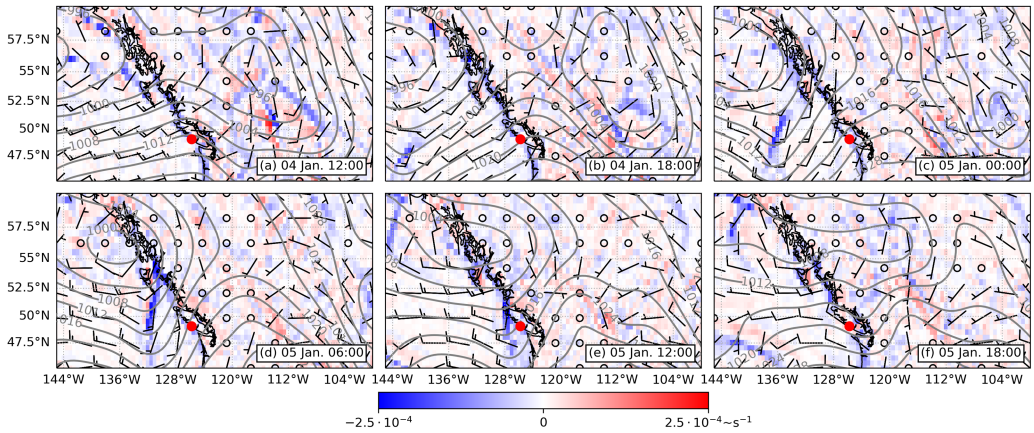

Fig. 6. Surface wind (10 m, barbs, knots) and isobars (each 4 hPa) forecast by GFS on January 4–5, 2020, along with divergence of the horizontal wind velocity field (color scale, s^{-1}). The red dot is the location of Tofino.

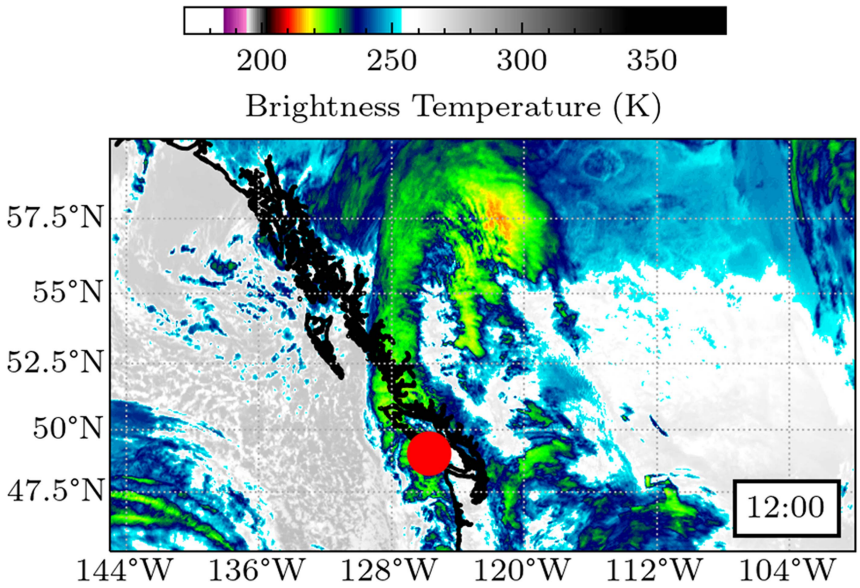

Fig. 7. Infrared satellite image (1×1 km resolution) captured by GOES-17 ABI in band 13 (10.3 μm) at 12:00 UTC on January 5, 2020.

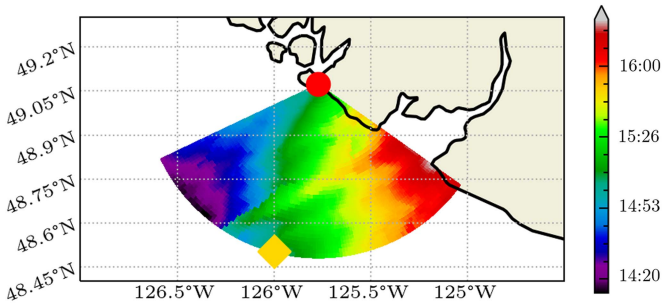

Fig. 8. Cold front arrival times (color scale, UTC) derived from GOES-17 cloud tops brightness temperature Tb.

each GOES-17 pixel within the radar sweep area. We derived the time of arrival using time series of brightness temperature of the cloud tops for each pixel between 14:00 and 16:00 (see Fig. 8). Using these arrival times, we could infer an average propagation speed of 15.8 m·s^{-1} and an eastward propagation direction. It is worth noticing that the atmospheric disturbance propagated in the same direction as the disturbance observed by the WERA radar and has comparable arrival times.

D. HF Radar Wind Data

Early work on extracting wind directions from HF ocean radar was carried out [18] using sky-wave radars and was developed further for ground-wave systems [19], [20] among many others.

The energy in the two first-order peaks in an HF radar Doppler spectrum of ocean echoes is determined by the wave heights of resonant Bragg waves in the wind-wave spectrum that are propagating in the radial directions (±) of the radar beam. For example, if the wind is directed toward the radar then the wind waves will be at a maximum in the radial direction toward the radar and very small in the upwind direction away from the radar. In this case, the ratio of the first-order peak energies will be very large. This is illustrated in Fig. 9(a), which

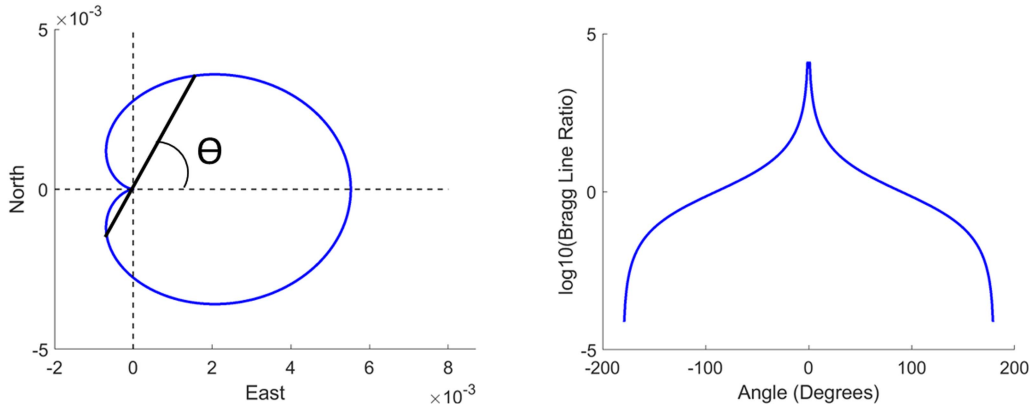

Fig. 9. Left panel is the wind directional spectrum model $G(\theta)$. The black line represents the direction of the narrow beam of the radar. The ratio $G(\theta)/G(\theta+\pi)$ is in the right panel.

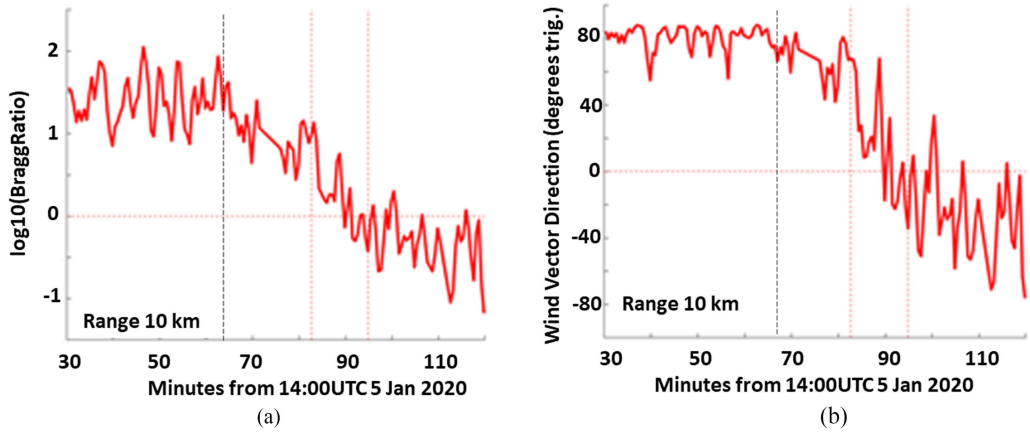

Fig. 10. Radar data at range 10 km, directly south of the radar station. (a) Ratio of first-order peaks. (b) Deduced wind directions using the model. The red dashed lines mark the radar alert period and the black dashed line marks the commencement of the wind shift.

uses the spreading term in a model for the directional spectrum of wind-waves given by Longuet-Higgins et al. [21]. The ± ambiguity in HF radar wind direction is resolved by a nearby anemometer or synoptic predictions for the area.

The blue curve in Fig. 9(a) is calculated using

$$G\ (\theta) = A\cos^{2s}\left(\theta/2\right) \tag{6}$$

where A is a normalizing factor to make $\int_0^{2\pi} G(\theta)d\theta = 1$. The angle θ is measured from the direction of the wind that, for convenience in the illustration, we have taken to be eastwards.

Fig. 9 has $s = 1$, which makes the curve a cardioid.

The ratio of spectral energies is $R = G(\theta)/G(\theta+\pi)$, which is plotted in Fig. 9(b) as $\log_{10} R$. The Longuet-Higgins model, with various values of s, has been used by several authors to produce wind direction, θ, from the ratio R measured by the HF radar (for example [22]). This procedure has limitations due to assumptions of the model. Specifically, in the case where R is large [θ near zero in (5)], the conversion from R to θ is poorly conditioned. Alternative models for $G(\theta)$ remove the cusp at $\theta = 0$.

An improved method has been developed [23] for deriving wind directions from the ratios of energy in the Bragg lines. However, in this article, we are concerned mainly with the timing of changes in the wind direction rather than the actual directions. For that reason, we are using $\log_{10}(R)$ as a metric of wind shifts. Fig. 10 illustrates the relationship between $\log_{10}(R)$ and θ for data from the Tofino radar using the Longuet-Higgins model. $\mathrm{Log}_{10}(R)$ is constant up to 15:02 h at which time it starts to shift toward zero. The interpretive model for wind direction, θ [Fig. 10(b)], is poorly conditioned for northward wind, whereas the directly measured parameter R has consistent precision when expressed logarithmically in Fig. 10(a). The wind direction at the 10 km range starts to move from near northwards about 20 min before the start of the radar alert period and reaches eastwards during that period. Fig. 10(b) demonstrates the varying precision of the direction estimate, contrasting with the consistency in precision of the $\log_{10}(R)$ parameter in Fig. 10(a).

Wind direction data are available from the WERA HF radar at individual grid points every 33 s with a time resolution of 133 s.

IV. WERA Radar as a Real-Time Monitor

The main features of the change in oceanographic conditions around 15:00 h–16:00 h on January 5, 2020 at Tofino are the surface currents and the wind direction and these results are available from the HF radar alone as a real-time monitor. In this case, where there is a single radar station the currents measured are in the direction of the radials toward the station. Figs. 11–13 show these features in a time period that includes that of the real-time alert issued by the WERA radar. The

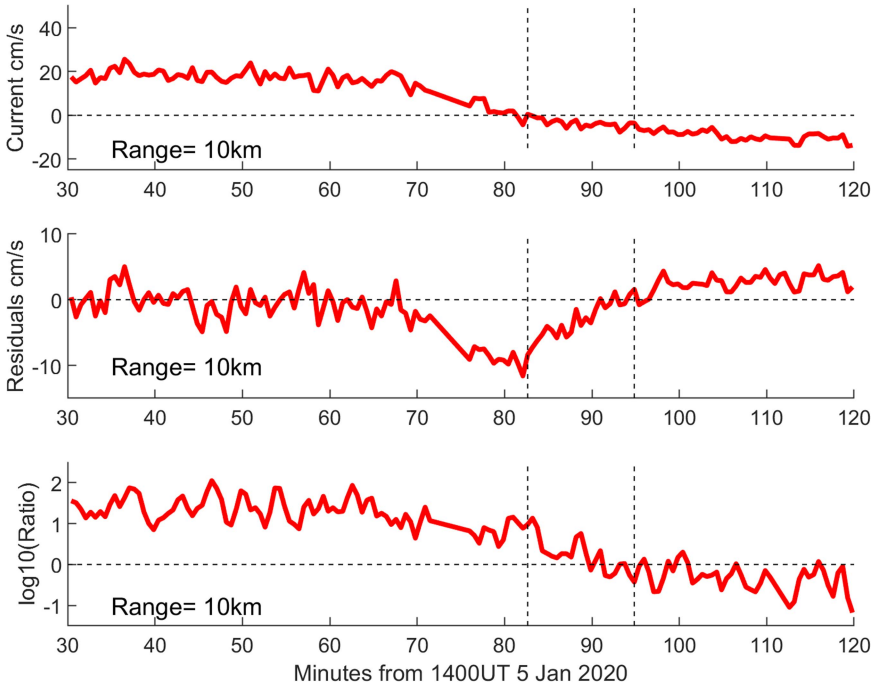

Fig. 11. WERA radar observations at 10-km range, with the radar beam looking southwards. The vertical dashed lines mark the period of the real-time disturbance alert.

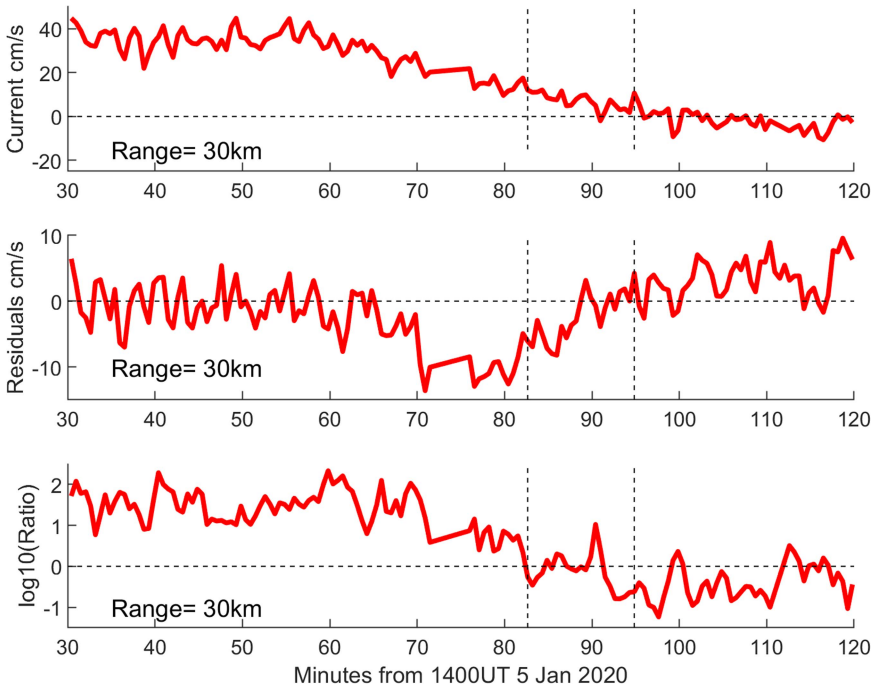

Fig. 12. WERA radar observations at 30-km range, with the radar beam looking southwards. The vertical dashed lines mark the period of the real-time disturbance alert.

data plotted in these figures are from the HF WERA radar at grid points directly south of the radar at ranges 10, 30, and 50 km and are averages for each parameter over the 3 × 3 matrix of grid points centered on the nominated point.

The commencement of the southward current flow averaged over 10–50-km range was at 14:59:36 h UT (±4.4 min), which is consistent with the high water at the Tofino tide gauge at 14:52 h. The commencement of the residual anomaly averaged over 10–50-km range was at 15:06:50 (±2.5 min), which is consistent with the peak in the surge at the Tofino tide gauge at 15:06 h. The commencement of the wind shift averaged over 10–50-km range was at 15:06:36 h (±3.4 min).

The coincidence of the commencement of the southwards current flow and the wind shift suggests that the relaxation of the wind-driven setup following the easing of the northwards wind was the

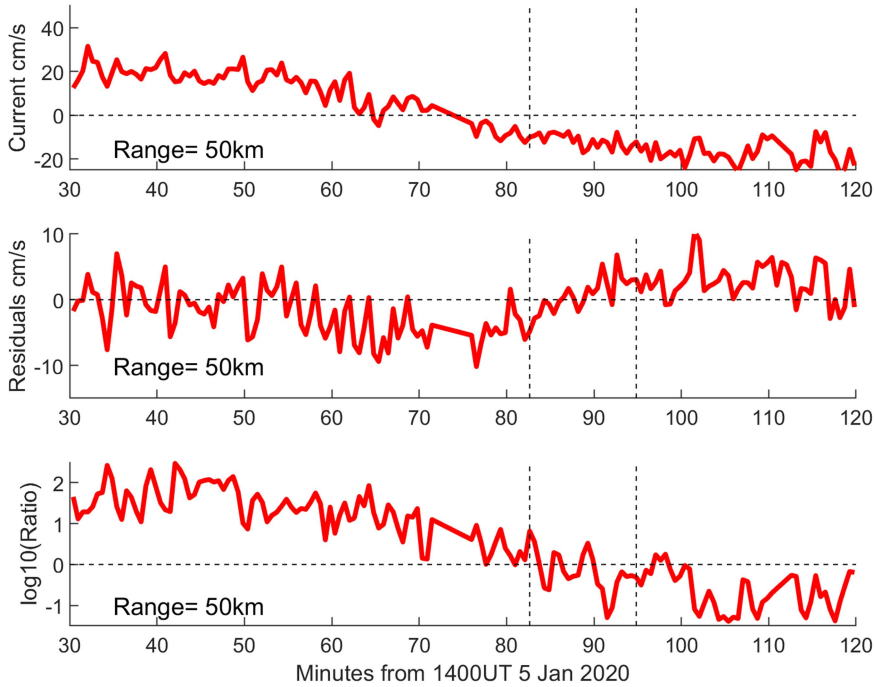

Fig. 13. WERA radar observations at 50-km range, with the radar beam looking southwards. The vertical dashed lines mark the period of the real-time disturbance alert.

cause of the southwards anomaly in the residual current as the setup relaxed.

The four oscillations evident in radar PT data in Fig. 2 that follow the main disturbance have an average period of approximately 24 min. This is roughly consistent with the fluctuations in the tide gauge data in Fig. 4(c), which have an average period of 29 min. Analysis of the radar currents revealed no propagating wave in this sequence and the oscillations are most likely due to seiching in the complex inland waterways.

V. Discussion

The phase speed of tsunamis propagating from the deep ocean toward the shore reduces as the water depth decreases (2). This produces a strong refraction effect such that one can assume that a tsunami with distant genesis will be propagating perpendicularly to the bathymetry contours. It is only locally generated tsunamis that might be observed propagating in any other direction. The question about the Tofino event on January 5, 2020 is whether it could have been a meteotsunami generated locally.

Figs. 11–13 show that the anomaly in the northwards component of surface current of about –10 cm·s^{-1} lasted for about 20 min. For a tsunami with maximum surge velocity v_m in water depth d, the amplitude is given by (4) in Section II.

For $v_m = 0.10$ m·s^{-1} and $d = 50$ m, a tsunami would have a water elevation of 0.22 m at 30-km range at Tofino, increasing as the tsunami propagated toward the shore. This would have been a minor tsunami of around half a meter at the coast, typical of a meteotsunami [24]. Based solely on residual current data in real time, the tsunami in detection software issued the alert.

However, other data and calculations alter this conclusion. The average west-east speed of the disturbance in postanalysis of the radar data was 17.0 ± 3.2 m·s^{-1}, and from the GOES-17 satellite data 15.8 m·s^{-1}. A tsunami propagating as a shallow water gravity wave at this speed would require water depth of about 27 m (2). This depth exists only a few kilometer from shore at Tofino (see Fig. 1), indicating that the disturbance propagating in the west-east direction would not be a tsunami gravity wave.

Furthermore, for a gravity wave propagating in the west-east direction, the rotational velocity of the water parcels would be in the vertical west-east plane and the surface surge velocities directed west-east, with no component along the north–south axis. The HF radar at Tofino observed an west-east propagating disturbance with significant surge current components on the north-south axis, which is not consistent with it being a tsunami gravity wave.

The alert issued at Tofino on January 5, 2020 was for a wind-driven event where the northwards wind over several hours produced an anomalous high-water setup at the tide gauge. With the arrival of a cold front, the onshore component of wind dropped significantly (due mainly to wind shift) and the water setup relaxed to produce an anomalous pulse of water away from the shore over about a 20-min period.

It is possible that the pulse of water could have satisfied the Proudman resonance condition [25] near to the coast. While that is not indicated by the data, these are the conditions for a weak meteotsunami to be generated close to the coast and, if so, would propagate in a south-easterly direction.

In this case study, the WERA HF radar has issued an alert for a disturbance in surface currents that had the characteristics of a minor tsunami event. Data from the meteorological and tidal observations show that it was not a tsunami but a wind-driven disturbance. The wind direction parameter combined with the surface current data from the radar has the potential to differentiate between tsunami and wind surge events in real time. An abrupt change in wind direction at the time of tsunami-like surface currents could be implemented in HF radar tsunami alert software.

References

[1] H. Roarty et al., "The global high frequency radar network," *Front. Mar. Sci.*, vol. 6, 2019, Art. no. 164, doi: 10.3389/fmars.2019.00164.

[2] J. D. Paduan, "Oceanographic applications of high-frequency (HF) radar backscatter," in *Ocean Remote Sensing Technologies: High Frequency, Marine and GNSS-Based Radar*, W. Huang and E. W. Gill, Eds., London, U.K.: Inst. Eng. Technol., 2021.
[3] L. R. Wyatt, J. J. Green, and A. Middleditch, "HF radar data quality requirements for wave measurement," *Coastal Eng.*, vol. 58, pp. 327–336, 2011, doi: 10.1016/j.coastaleng.2010.11.005.
[4] B. Lipa et al., "High frequency (HF) radar detection of the weak 2012 Indonesian tsunamis," *Remote Sens.*, vol. 4, pp. 2944–2956, 2012.
[5] A. Dzvonkovskaya, D. Figueroa, K.-W. Gurgel, H. Rohling, and T. Schlick, "HF radar WERA observation of a tsunami near Chile after the recent great earthquake in Japan," in *Proc. Int. Radar Symp.*, Leibzig, Germany, 2011, pp. 125–130.
[6] B. Lipa et al., "Japan tsunami current flows observed by HF radars on two continents," *Remote Sens.*, vol. 3, pp. 1663–1679, 2011, doi: 10.3390/rs3081663.
[7] B. Lipa, D. Barrick, and J. Isaacson, "Coastal tsunami warning with deployed HF radar systems," in *Tsunami*, vol. 73, M. Mokhtari, Ed. Rijeka, Croatia: InTech, 2016, ch. 5, doi: 10.5772/63960. Online. Available: http://www.intechopen.com/books/tsunami/coastal-tsunami-warning-with-deployed-hf-radar-systems
[8] K.-W. Gurgel, A. Dzvonkovskaya, T. Pohlmann, T. Schlick, and E. Gill, "Simulation and detection of tsunami signatures in ocean surface currents measured by HF radar," *Ocean Dyn.*, vol. 61, pp. 1495–1507, 2011, doi: 10.1007/s10236-011-0420-9.
[9] A. Dzvonkovskaya, "HF surface wave radar for tsunami alerting: From system concept and simulations to integration into early warning systems," *IEEE Aerosp. Electron. Syst. Mag.*, vol. 33, no. 3, pp. 48–58, Mar. 2018.
[10] A. Dzvonkovskaya, L. Petersen, and T. Insua, "Real-time capability of meteotsunami detection by WERA ocean radar system," in *Proc. 8th Int. Radar Symp.*, Prague, Czech Republic, 2017, pp. 28–30.
[11] C.-A. Guérin, S. T. Grilli, P. Moran, A. R. Grilli, and T. L. Insua, "Tsunami detection by high-frequency radar in British Columbia: Performance assessment of the time-correlation algorithm for synthetic and real events," *Ocean Dyn.*, vol. 68, no. 4/5, pp. 423–438, 2018.
[12] M. Heron, "The role of HF ocean surface radar in Australia as a long-term coastal ocean monitoring facility," in *Proc. 17th Australas. Coastal Ocean Eng. Conf./10th Australas. Port Harbour Conf.*, 2005, pp. 185–190.
[13] G. Green, "On the motion of waves in a variable canal of small depth and width," *Math. Papers Late George Green(Cambridge Library Collection - Math.*, N. Ferrers, Ed., Cambridge, U.K.: Cambridge University Press, pp. 223–230, 2014, doi: 10.1017/CBO9781107325074.007.
[14] B. Kinsman, *Wind Waves*. Englewood Cliffs, NJ, USA: Prentice-Hall, 1965.
[15] J. Gower, "The 26 December 2004 tsunami measured by satellite altimetry," *Int. J. Remote Sens.*, vol. 28, pp. 2897–2913, 2007, doi: 10.1080/01431160601094484.
[16] M. L. Heron, "HF radar in tsunami detection," in *Ocean Remote Sensing Technologies: High Frequency, Marine and GNSS-Based Radar*, W. Huang and E. Gill, Eds., London, U.K.: Inst. Eng. Technol., 2021, ch. 9.
[17] B. Domps, J. Marmain, and C.-A. Guérin, "A reanalysis of the October 2016 "Meteotsunami" in British Columbia with help of high-frequency radars and autoregressive modeling," *IEEE Geosci. Remote Sens. Lett.*, vol. 19, 2022, Art. no. 3505105.
[18] A. E. Long and D. B. Trizna, "Measurements and preliminary interpretation of HF radar Doppler spectra from the sea-echo of an Atlantic storm," Nav. Res. Lab., Washington, DC, USA, Rep. 7456, 1972.
[19] M. Heron and R. Rose, "On the application of HF ocean radar to the observation of temporal and spatial changes in wind direction," *IEEE J. Ocean. Eng.*, vol. OE-11, no. 2, pp. 210–218, Apr. 1986.
[20] D. M. Fernandez, H. C. Graber, J. D. Paduan, and D. E. Barrick, "Mapping wind directions with HF radar," *Oceanography*, vol. 10, pp. 93–95, 1997, doi: 10.5670/ocenog.1997.33.
[21] M. S. Longuet-Higgins, D. E. Cartwright, and N. D. Smith, "Observations of the directional spectrum of sea waves using the motions of a floating buoy," in *Ocean Wave Spectra*. Englewood Cliffs, NJ, USA: Prentice-Hall, 1963, pp. 111–136.
[22] L. R. Wyatt, L. J. Ledgard, and C. W. Anderson, "Maximum likelihood estimation of the directional distribution of 0.53 Hz ocean waves," *J. Atmos. Ocean. Technol.*, vol. 14, no. 3, pp. 591–603, 1997.
[23] W. Shen and K.-W. Gurgel, "Wind direction inversion from narrow-beam HF radar backscatter signals in low and high wind conditions at different frequencies," *Remote Sens.*, vol. 10, 2018, Art. no. 1480, doi: 10.3390/rs10091480.
[24] I. Vilibić et al., "Atmospheric processes responsible for generation of the 2008 Boothbay meteotsunami," *Natural Hazards*, vol. 74, pp. 25–53, 2014, doi: 10.1007/s11069-013-0811-y.
[25] J. Proudman, "The effects on the sea of changes in atmospheric pressure," *Geophys. J. Int.*, vol. 2, pp. 197–209, 1929, doi: 10.1111/j.1365-246X.1929.tb05408.x.

Mal Heron (Life Fellow, IEEE) received the Ph.D. degree in radio science from the University of Auckland, Auckland, New Zealand, in 1971.

From 1971 to 2007, he had an Academic career with James Cook University, Douglas, QLD, Australia, where he is currently an Adjunct Professor of physics. From 2007 to 2012, he was the Foundation Director of the Australian Coastal Ocean Radar Network. He is also a semiretired Consultant with Portmap Remote Ocean Sensing Pty Ltd., Townsville, QLD, Australia. His interests include research in coastal oceanography and the development and applications of HF ocean surface radar.

Dr. Heron is currently an elected member of IEEE-OES AdCom.

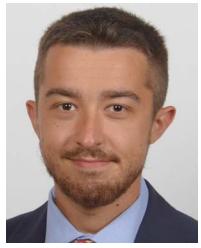

Baptiste Domps received the B.Eng. degree in microwave engineering from Bordeaux INP, Bordeaux, France, in 2018, and the Ph.D. degree in physics of remote sensing from the University of Toulon, Toulon, France, in 2021.

He is a Radar Systems Engineer with Degreane Horizon (VINCI Group), Cuers, France. He currently focuses on the design of methods and systems for the radar probing of the sea surface and the atmosphere.

Dr. Domps was the recipient of the 2022 "Admiral Daveluy Prize" by the French Navy for his Ph.D. research.

Charles-Antoine Guérin received the Ph.D. degree in theoretical physics from the University of Aix-Marseille, Toulon, France, in 1998.

He is currently a Professor with the Mediterranean Institute of Oceanography, University of Toulon, Toulon. His research interests include ocean remote sensing with microwave and high-frequency radars.

Manman Wang received the master's degree in physical oceanography from the University of Victoria, Victoria, BC, Canada, in 2016.

She is currently a Junior Staff Scientist with the Ocean Networks Canada, which is an ocean observing facility hosted and owned by the University of Victoria, and delivers ocean data from its cabled, mobile, and community-based observing networks. Her research interests include dynamics in coastal oceanography, mixing, turbulence, as well as the quality and application of HF radars.

Leif Petersen received the Diploma in electrotechnical engineering from the Christian Albrechts University, Kiel, Germany, in 2024.

He then directly joined Helzel Messtechnik GmbH, Kaltenkirchen, Germany, as Project and Development Engineer. He is currently the Managing Director with Helzel Messtechnik GmbH, the company building the oceanographic WERA HF radar system and the Helzel OTHR system to monitor the EEZ. His research interests include measurement hardware and renewable energies.